A Hierarchical Economic Model Predictive Controller That Exploits Look-Ahead Information of Roads to Boost Engine Performance

Liu, Z., Dizqah, A. M., Herreros, J. M., Schaub, J. & Haas, O.

A Hierarchical Economic Model Predictive Controller That Exploits Look-Ahead Information of Roads to Boost Engine Performance

Zihao Liu[ID], Arash M. Dizqah[ID], *Member, IEEE*, Jose M. Herreros[ID], Joschka Schaub,
and Olivier C. L. Haas[ID], *Senior Member, IEEE*

Abstract— Sensors and communication capabilities of connected vehicles provide look-ahead information that can be exploited by vehicle controllers. This work demonstrates the benefits of look-ahead information combined with hierarchical economic model predictive control for the airpath management of compression ignition engines. This work exploits road information predicted with a 0.1- and 2-s horizon to simultaneously control fast and slow engine dynamics, respectively. It controls the variable nozzle turbocharger and dual-loop exhaust gas recirculation, at a 0.01-s rate, to simultaneously optimize NOx, soot, and fuel economy. Simulation studies and hardware-in-loop implementation on an ARM Cortex-A15 processor demonstrate improved NOx, soot, and torque tracking without compromising fuel economy, and a worst case computation time of 8.92 ms.

Index Terms— Airpath control, economic model predictive controller (eMPC), exhaust gas recirculation (EGR), look-ahead control, model predictive control (MPC), variable nozzle turbocharger (VNT).

NOMENCLATURE

BSFC	Brake specific fuel consumption.
CAN	Controller area network.
CI	Compression ignition.
DOC	Diesel oxidation catalyst.
DPF	Diesel particulate filter.
EATS	Exhaust aftertreatment system.
ECU	Electronic control unit.
EGR	Exhaust gas recirculation.
eMPC	Economic model predictive controller.
HeMPC	High-level eMPC.
HiL	Hardware-in-the-loop.
HP	High pressure.
LAeMPC	Look-ahead eMPC.
LeMPC	Low-level eMPC.
LP	Low pressure.
LUT	Lookup table.
MPC	Model predictive control.
NMPC	Nonlinear model predictive controller.
NPD	Nonpositive definite.
OCP	Optimal control problem.
OFR	Oxygen fuel ratio.
PI	Proportional–integral.
PID	Proportional–integral–derivative.
RMSE	Root-mean-square error.
SCR	Selective catalyst reduction.
SD	Standard deviation.
VNT	Variable nozzle turbocharger.
WLTC	Worldwide harmonized light vehicles test cycles.
I	Identity matrix.
$N_{\{\cdot\}}$	Diagonal matrix containing scaling factors to normalize objective function terms.
$Q_{\{\cdot\}}$	Diagonal matrices containing nonnegative weightings for objective function terms.
λ_O	Ratio between oxygen fuel ratio and its stoichiometric value.
$\{\cdot\}_H, \{\cdot\}_L$	Variables related to HeMPC and LeMPC, respectively.
$\{\cdot\}_{\text{mea}}, \{\cdot\}_{\text{est}}$	Measured and estimated variables, respectively.
bmep	Brake mean effective pressure.
$l_{\{\cdot\}}$	Stage cost function.
$M_{\text{air}}, M_{\text{o2}}$	Molar mass of air and oxygen.
$m_{\text{cyl}}, m_{\text{fuel}}$	Cylinder mass intake and mass fuel injection per stroke, respectively.
$n_{\{\cdot\}}$	Prediction horizon.
ne	Engine rotary speed.
p_2, p_{loss}	Intake manifold pressure and pumping loss, respectively.
T_2, T_{co}	Intake manifold and coolant temperature, respectively.
$t_s, t_{\{h,l,v\}}$	Sampling time and valve time constant of {HP EGR, LP EGR, VNT}, respectively.
$u_{\{h,l,v\}}, \tilde{u}_{\{h,l,v\}}$	Commanded and actual valve position of {HP EGR, LP EGR, VNT}, respectively.
$u_{v,\text{eff}}$	Most efficient variable nozzle turbocharger valve position (operating point specific).

w	Scaler weightings of objective function terms.
x_O, x_{nox}, x_{soot}	Cylinder oxygen concentration before combustion, cylinder NOx, and soot concentration after combustion, respectively.
OFR, OFR$_{stoich}$	Oxygen fuel ratio and stoichiometric oxygen fuel ratio, respectively.

I. INTRODUCTION

THE airpath system in CI engines involves complex coupled and nonlinear dynamics of intake manifold pressure (also known as boost pressure) and in-cylinder oxygen concentration [1]. A typical airpath control design aims to meet conflicting performance objectives, including driveability (i.e., torque tracking), fuel economy, and emissions via regulating the VNT and EGR valves. The control of VNT and EGR decides the boost pressure and in-cylinder oxygen concentration. The use of EGR reduces oxygen concentration, which lowers NOx at costs of higher soot emissions, known as the NOx–soot tradeoff [2]. The control of VNT adjusts boost pressure, which dictates the total mass of combustion charge. Higher boost pressure requires more energy from the exhaust gas and results in greater fuel consumption but better torque tracking [3]. Ensuring good tracking also conflicts with emission objectives since the use of EGR reduces oxygen mass available for combustion and can cause pressure loss at exhaust manifold, leading to reduced energy input to the VNT.

The abovementioned coupled dynamics and conflicting objectives require dedicated calibration methodologies for airpath control [4], [5] to meet legislative and performance requirements. Industrial applications typically follow a model-based approach [1] to find the desired operating points of boost pressure and in-cylinder oxygen concentration for a set of engine steady-state operating conditions. The corresponding control utilizes model-based feedforward control with the desired operating points fulfilled by some reactive feedback controller [6]. Using feedforward and reactive tracking control including PI/PID [7], H_∞ [8] allows direct use of inverse engine models that are nonlinear and discontinuous with empirically determined parameters. The resulting controllers, however, cannot systematically handle the underlying multivariable dynamics together with operating constraints such as OFR limit.

MPC-based [9] controllers have become prominent for the use in CI engines [10]. The approach of MPC formulates the multivariable process dynamics and constraints into an OCP, solved by dedicated optimization algorithms [11]. Huang et al. [12] presented a rate-based and gain-scheduled MPC that uses a single linear engine model to track set points of boost pressure and EGR fraction. The resulting controller demonstrates promising execution efficiency for ECUs and has shown good tracking performance. Another tracking MPC in [13] is experimentally validated on a 13-L engine but requires 192 linear models. Sankar et al. [14] presented a robust MPC with recursive feasibility guarantee using 12 linear

engine models. Nonlinear MPC allows fewer models, hence avoiding frequent model switching, as well as convenient consideration of nonlinear states including emissions, at costs of higher computational costs. Liao-McPherson et al. [15] presented an NMPC for the tracking of airpath set points and reported an estimated worst case execution time of 1.73 ms on a 256-MHz ECU. Using a supervisory MPC that acts as a reference governor to limit soot emissions and enforce fuel-to-air ratio constraints, Liao-McPherson et al. [15] demonstrated emission reduction for a slight increment in fuel consumption compared to an industrial benchmark controller over the WLTC. Moreover, MPC can track objectives while constraining emissions and fuel economy [14], [16] or act to modify tracking references by considering emission and engine protection constraints [17].

The so-called eMPCs [9] offer advantages in terms of the required calibration because they calculate the optimum operating point directly and do not require prior knowledge of the set points to be tracked. Liao-McPherson et al. [18] presented an eMPC that maximizes engine efficiency while minimizing torque tracking error and constraining NOx emissions over a horizon of 1.5 s. The resulting eMPC computes the optimal set points for an inner tracking controller. Liu et al. [19] presented an eMPC that directly controls the EGR and VNT valves with simultaneous consideration of NOx, soot emissions, fuel economy, and torque tracking. The approach of eMPC optimizes the performance objectives considering the engine dynamics and can discover operating points that allow better transient performance and constraint satisfaction than a conventional set-point tracking control scheme where set points are decided on a steady-state basis.

The ability of MPC to consider performance objectives over a time horizon is frequently associated with "look-ahead control" or "control with preview," where future (i.e., look-ahead) information fills its prediction horizon. This motivates the research question on how look-ahead information can improve the performance of MPC-based airpath controller. The look-ahead information can be future road information and speed planning trajectory that is made accessible by vehicle connectivity [20] and sensors, including lidars [21] and cameras [22]. The corresponding "look-ahead control" has been applied to energy-efficient cruise control [23], road intersection utilization improvement [24], ride comfort enhancement [25], and fuel cell management [26]. The MPC in [27] plans gear shifting and longitudinal vehicle dynamics to maximize fuel economy while constraining NOx emissions. However, the benefits of look-ahead information were not reported. Similarly, in [28] where energy–emission tradeoff is studied under eco-following scenarios for connected automated vehicles, the difference in using look-ahead information is not analyzed. Velmurugan et al. [29] used a 60-s "look-ahead" for aftertreatment control to calculate the optimal engine-out NOx set points to minimize fuel and urea consumption while ensuring legislative-compliant tailpipe emissions. Reduced fuel and urea costs are achieved at the cost of increasing tailpipe NOx emissions, with an overall 0.98% reduction in the total objective function value.

Applications of look-ahead control commonly utilize a long horizon at tens of seconds or greater. The airpath control, however, is a hard real-time problem at a milliseconds scale. To harvest the most benefits from look-ahead information, the horizon should ideally be as long as possible, making real-time application of airpath MPC more challenging and not seen in the current literature. To reduce computation burden, Gelso and Dahl [13], [16], and Liao-McPherson [18] reduced the number of decision variables via move-blocking that forces control variables to remain constant for a given set of prediction steps. Huang et al. [12] suggested that specialized constraint treatment can be employed in the optimization routine. Norouzi et al. [30] and Moriyasu et al. [31] employed deep learning and neural approximation-based modeling of optimal control laws of MPC, demonstrating significantly shorter execution time. The approximated control law, however, requires retraining of the model for each change in control design. To accommodate the presence of different timescales within the engine dynamics, multivariable airpath control may be decoupled using hierarchical or cascade control designs. Umezawa et al. [32] analyzed the time horizons of coupled control problems and utilized hierarchical MPC to efficiently accommodate OCPs of the long and short horizons. Another hierarchical MPC in [33] uses its high-level component to account for road data offline, whereas a low-level controller operates in real time to compute the desired powertrain operating parameters. This work stems from the benefits of eMPC in terms of reduced controller calibration effort and the ability to exploit look-ahead information relating to the expected vehicle speed profile based on its predicted path. Different from the eMPC in [19], this work exploits and demonstrates the benefits of look-ahead information to improve the control of airpath. To additionally harvest the look-ahead information, this work uses a hierarchical control design, whereas a single eMPC is used in [19] to accommodate both slow and fast dynamics. The contributions of this article are given as follows.

1) Demonstrate that an engine airpath controller using look-ahead information can simultaneously improve torque tracking, engine-out NOx, and soot emissions by, respectively, 11.1%, 5.3%, and 11.5% compared to a similar controller without any such preview information.
2) Propose a novel, computationally efficient hierarchical eMPC with a multirate structure to optimally control the airpath of the engine using the look-ahead information of engine speed and torque demand. The controller is shown to be resilient to both delay and magnitude uncertainties in look-ahead information.
3) Real-Time implementation of the proposed hierarchical eMPC operating on an HiL test platform, highlighting the opportunity for deployment on production vehicles.

This article is organized as follows. Section II describes the EURO 6 engine used for this study, its experimentally validated model, and the controllers evaluated. Section III presents the look-ahead horizon determination, the controller design, and the formulation of the OCP. Section IV details
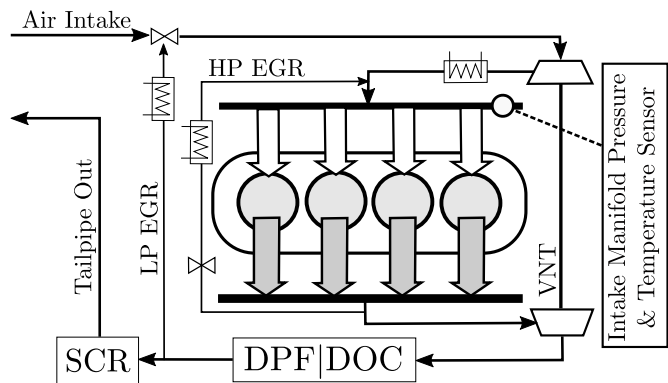

Fig. 1. Schematic of EURO 6 2L four-cylinder turbocharged CI engine with dual-loop EGR and VNT. Unused sensors are not shown, including air mass flow filter, temperature, and pressure sensors within EATS.

the experimental implementation for the controllers. Section V describes and critically evaluates the simulation studies and HiL implementation. Section VI concludes this article and suggests future works.

II. SYSTEM AND BENCHMARK CONTROLLERS

Fig. 1 shows the target engine used for this work. The model of the target engine, provided by FEV GmbH, was experimentally validated in [34] and [35] and follows a mean value approach of 0.01-s resolution. It uses physics-based models of flow, combustion, and heat transfer with empirically determined model parameters stored in LUTs. The dual-loop EGR system includes an LP EGR with its valve located upstream of the compressor. In contrast, the HP EGR directly connects the exhaust manifold to the intake manifold. An EATS is available downstream the VNT, consisting of a DOC, DPF, and SCR. This investigation, however, concentrates on engine-out emissions. Two controllers are used for performance benchmarking: 1) a EURO 6 production-line controller including control of airpath, injection (mass and timing), common rail pressure, and EATS (see Fig. 2) [35], [36] and 2) an economic MPC using 0.1-s horizon without look-ahead information [19]. This work develops an LAeMPC that shares similar objectives to the eMPC [19] but with a longer horizon of look-ahead information. The resulting performance difference of the LAeMPC against the eMPC implies the potential advantage of using look-ahead information. Compared to the eMPCs, the production-line controller is reactive and employs a combination of feedforward and PI/PID [35], [36].

ECUs typically run injection control at fixed crank angle intervals but with variable sampling rates. This work adopts a fixed rate of 0.01 s for simplicity. All controllers exploit sensor information available on production engines, including an engine speed sensor, a coolant temperature sensor, and an integrated pressure and temperature sensor at the intake manifold. The LUTs in the production-line controller are used in this work for the feedforward estimation of cylinder oxygen concentration and brake torque. The look-ahead information includes the engine speed and torque.
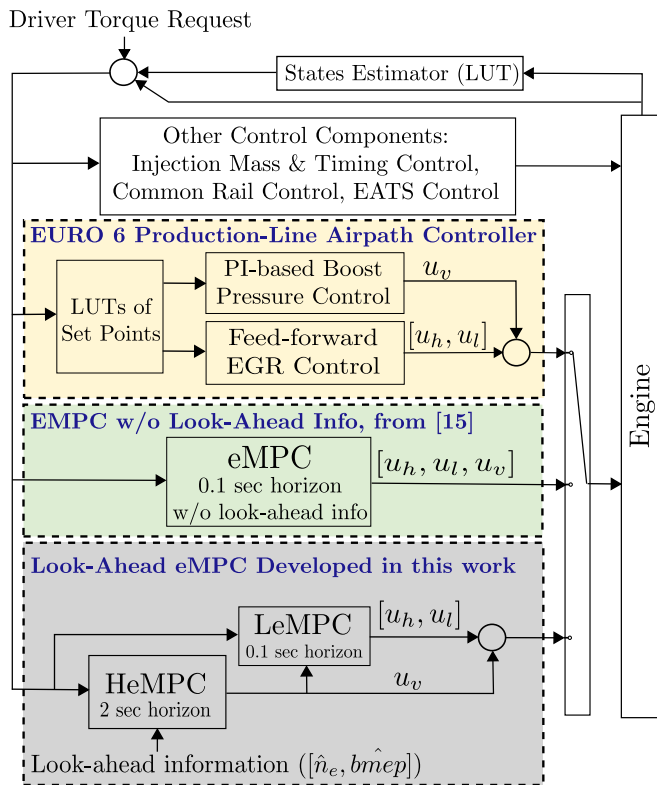
Fig. 2. Illustration of the three airpath controllers evaluated in this work is enclosed in the dashed boxes. Only one of the controllers is enabled at one time by a selector. The other engine control components are provided by the production-line controller.
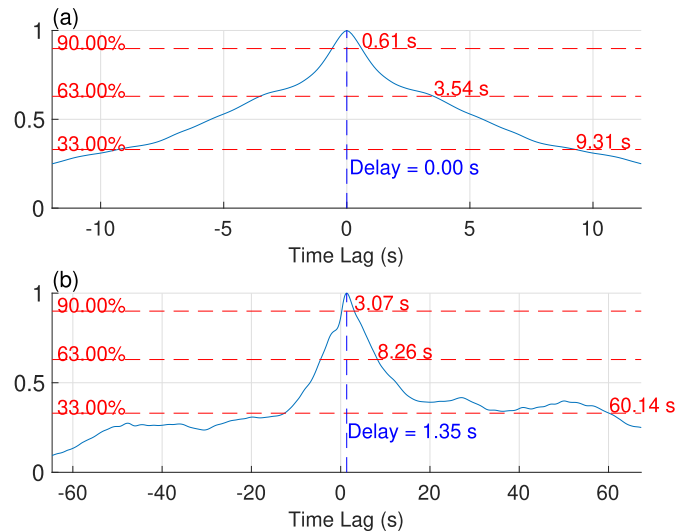

Fig. 3. (a) Autocorrelation of torque of the WLTC, which identifies that a 3.5-s horizon provides useful information. (b) Cross correlation of boost pressure and torque in the WLTC, which identifies the turbo-lag of 1.4 s and up to 8.3-s time lag of strong correlation.

III. CONTROLLER DESIGN

The future engine speed and torque demand, used as look-ahead information for this work, are not directly available but depend on the vehicle configurations (i.e., mass and powertrain parameters) and driving mode/policy. With speed predictor algorithms such as [37], [38], and [39] to take account of traffic and road elevation and knowledge of vehicle parameters, the engine speed and torque of a predicted speed profile of a given vehicle can be calculated deterministically. This work does not delve into this conversion and assumes that the look-ahead information of engine speed and torque demand is readily available.

A. Choice of Look-Ahead Horizon

The choice of controller look-ahead horizon is a tradeoff between the quantity of look-ahead information, relevant system dynamics, and computational requirements. The velocity profile of WLTC is used to evaluate the quantity of look-ahead information. However, similar approaches can be adopted for other drive cycles, combinations of drive cycles, or driving modes, e.g., "sport" and "eco." The torque demand is found to be more correlated to the velocity profile than the engine speed. The autocorrelation of torque demand [Fig. 3(a)] shows the relevance of past and future on the current torque demand. It is found that a time window of up to 3.5 s can provide exploitable information demonstrated by the high autocorrelation.

The dynamical behaviors of boost pressure and in-cylinder oxygen concentration are evaluated over step changes of EGRs and VNT. The VNT acts slowly on boost pressure with a settling time ranging from 1 to 4 s. In contrast, the HP EGR rapidly adjusts in-cylinder oxygen concentration under 0.1 s at any engine operating point. The settling time of in-cylinder oxygen using LP EGR is up to 0.5 s for medium-to-high engine loads and up to 1.5 s for low engine loads. In addition, the LP EGR uses a valve located upstream of the VNT compressor and immediately affects in-cylinder oxygen concentration without time delay. The step change of VNT has a negligible impact on in-cylinder oxygen concentration. The use of EGRs reduces the boost pressure to a greater extent as engine loading increases with a settling time of up to 1 s. Meanwhile, the HP EGR has a greater effect and longer settling time in reducing boost pressure than LP EGR. These findings suggest that the airpath dynamics of boost pressure and in-cylinder oxygen concentration have a time gap ranging from 0.1 to up to 4 s. Finally, the boost pressure is the slowest relevant dynamic. Its cross correlation to torque [see Fig. 3(b)] identifies a delay of 1.35 s corresponding to the turbo-lag. The impact of boost pressure on torque was found to be as long as 8 s.

Combining the velocity profile of WLTC and the corresponding airpath dynamics, a horizon of 3.5 s can exploit the engine load profile over WLTC, while a horizon between 1.4 and 8.0 s fully considers the airpath dynamics (including turbo-lag) and the impact of boost pressure on torque. However, to reduce the computational complexity, this study uses a 2-s look-ahead horizon, which corresponds to a sharp fall of torque autocorrelation in Fig. 3(a) and allows the consideration of turbo-lag in Fig. 3(b). Meanwhile, a 2-s horizon is in agreement with [18] and [40] who have demonstrated performance gains for airpath control and is within the 3-s (200 m ahead at 66.6 km/h) horizon for which a velocity prediction error around 5.7% was achievable [38].

B. Hierarchical EMPC Formulation

Using HP and LP EGRs, the oxygen concentration has a much faster dynamic at tens of milliseconds than boost pressure at seconds scale. The time difference in their respective dynamics motivates the use of hierarchical control with different horizons to account for look-ahead information while being computationally efficient. Fig. 2 shows the resulting LAeMPC that uses a low- and high-level eMPC to consider oxygen and boost pressure dynamics, respectively. The HeMPC exploits look-ahead information from engine speed and torque and uses a prediction step of 0.1 s to reach a 2-s horizon. It computes the optimal VNT positions while assuming that any oxygen value is feasible at 0.1-s interval. This assumption is valid since HP EGR can regulate oxygen concentration under 0.1 s and makes the oxygen value a manipulated variable for the OCP of HeMPC. The LeMPC adopts a prediction horizon of 0.1 s using a prediction step of 0.01 s without access to look-ahead information. It receives the optimal VNT position from HeMPC and computes the optimal EGR positions. Both HeMPC and LeMPC share the objectives to minimize pumping loss, NOx, and soot emissions, and both operate at 0.01 s. The HeMPC considers the impact of EGRs using the feedback values of boost pressure and in-cylinder oxygen concentration than explicitly the valve positions of EGRs. This simplifies the HeMPC to consider the optimal VNT control over a long (2 s) horizon of look-ahead information.

While the LP EGR has a longer settling time than HP EGR in terms of in-cylinder oxygen concentration, the LeMPC considers the same horizon of 0.1 s for both loops. This enables to meet the computational feasibility criteria but at the cost of higher use of HP EGR when a simultaneous fast control of in-cylinder oxygen concentration is desirable. At steadier and higher engine loadings, LAeMPC will gradually increase the share of LP EGR to reduce the pressure drop at the exhaust manifold leading to smaller pumping loss, hence better fuel economy. The dynamical difference between HP and LP may further benefit from look-ahead information and extended prediction horizon, but this is not considered in this work to achieve a reasonable online computation time.

Variables related to HeMPC and LeMPC use subscripts $(\cdot)_H$ and $(\cdot)_L$, respectively. Subscripts $(\cdot)_{\text{mea}}$ and $(\cdot)_{\text{est}}$ indicate measured and estimated values, respectively. Subscripts $(\cdot)_{\{h,l,v\}}$ denote variables related to HP EGR, LP EGR, and VNT, respectively. The diagonal matrix $\boldsymbol{T} = \text{diag}(t_h, t_l, t_v)$ contains the time constants of each valve. The base sampling time t_s is 0.01 s. $\boldsymbol{u}$ denotes $[u_h, u_l, u_v]^{\text{T}}$. $n_{(\cdot)}$ denotes prediction horizon. $y = [x_{\text{nox}}, x_{\text{soot}}, p_{\text{loss}}]^{\text{T}}$ contains the output states. Functions, unless with subscripts, are denoted in a generalized manner as $f(\cdot)$. $\rho = [\text{ne}, \text{bmep}]^{\text{T}}$ denotes the engine operating point. $\hat{\rho} = [\hat{\text{ne}}, \hat{\text{bmep}}]^{\text{T}}$ contains the future engine speed and torque demand that are assumed to be known.

The prediction models for in-cylinder NOx and soot concentrations, pumping loss, and cylinder air mass are given by

$$x_{\text{nox},k} = \exp(f_{\text{nox}}(p_{2,k}, x_{O,k}; \boldsymbol{\rho}_k)) \tag{1a}$$

$$x_{\text{soot},k} = \exp(f_{\text{soot}}(p_{2,k}, x_{O,k}; \boldsymbol{\rho}_k)) \tag{1b}$$

$$p_{\text{loss},k} = f(p_{2,k}, \tilde{\boldsymbol{u}}_k; \boldsymbol{\rho}_k) \tag{1c}$$

$$m_{\text{cyl},k} = f(p_{2,k}; \boldsymbol{\rho}_k) \tag{1d}$$

where the multiparametric polynomial functions $f(\cdot)$ and the corresponding identification method are described in [19]. The correlation between emissions (NOx and soot) and fuel quantity is captured using the brake torque and engine speed provided in $\boldsymbol{\rho}$, which, equivalently, considers total fuel energy and engine brake efficiency. The valve dynamics are identical in the plant and prediction model

$$\tilde{\boldsymbol{u}}_{k+1} = t_s \boldsymbol{T} \boldsymbol{u}_{k+1} + (\boldsymbol{I} - t_s \boldsymbol{T}) \tilde{\boldsymbol{u}}_k. \tag{2}$$

The dynamic states are modeled in (3). Boost pressure p_2 is identified at the sampling rates of 0.1 and 0.01 s for the high- and low-level eMPCs, respectively. The prediction model for HeMPC (3a) does not consider the use of EGRs. The effect of EGRs is considered by LeMPC in (3b)

$$p_{2,H,k+1} = f_H(p_{2,H,k}, x_{O,H,k}) + f_H(\tilde{u}_{v,k}; \boldsymbol{\rho}_k) \tag{3a}$$

$$p_{2,L,k+1} = f_{L,p_2}(p_{2,L,k}, x_{O,k}) + f_{L,p_2}(\tilde{\boldsymbol{u}}_k; \boldsymbol{\rho}_k) \tag{3b}$$

$$x_{O,k+1} = f_{L,x_O}(p_{2,L,k}, x_{O,k}) + f_{L,x_O}(\tilde{\boldsymbol{u}}_k; \boldsymbol{\rho}_k). \tag{3c}$$

λ_O is the fraction of OFR over its stoichiometric value $\text{OFR}_{\text{stoich}}$, where M_{o2} and M_{air} represent the molar mass of oxygen and air, and have constant values of 32 and 28.97 g/mol, respectively

$$\lambda_{O,k} = \frac{\left(m_{\text{cyl},k}\, x_{O,k}\, \frac{M_{\text{o2}}}{M_{\text{air}}}\right)}{m_{\text{fuel}}\, \text{OFR}_{\text{stoich}}}. \tag{4}$$

The OCP of the HeMPC and its stage cost function $l_{H,i}$ are as per (5) and (6), respectively

$$\underset{\boldsymbol{u}_v, \boldsymbol{x}_{O,H}}{\text{minimize}} \quad \sum_{i=1}^{n_H} l_{H,i}(\boldsymbol{y}_i, u_{v,i}; \boldsymbol{\rho}, \hat{\boldsymbol{\rho}}) \tag{5a}$$

$$\text{s.t. } (2), (1), (3a), (4) \tag{5b}$$

$$p_{2,0} = p_{2,\text{mea}}, \quad x_{O,0} = x_{O,\text{est}} \tag{5c}$$

$$\tilde{u}_{v,0} = \tilde{u}_{v,\text{mea}} \tag{5d}$$

$$\boldsymbol{u}_{v,\text{min}} \le \boldsymbol{u}_v \le \boldsymbol{u}_{v,\text{max}} \tag{5e}$$

$$\boldsymbol{x}_{\text{min}} \le \boldsymbol{x} \le \boldsymbol{x}_{\text{max}} \tag{5f}$$

$$\lambda_O \ge \lambda_{O,\text{min}}$$

$$k \in \{0, 1, \ldots, n_H - 1\} \tag{5g}$$

where

$$l_{H,i} := \alpha \times \left\{ (N_y y_i)^{\text{T}} Q_H (N_y y_i) \right.$$
$$+ w_{H,1}(N_{u_v}(u_{v,i} - u_{v,\text{eff}}))^2$$
$$\left. + w_{H,2}(N_{\Delta u_v} \Delta u_{v,i})^2 \right\} \tag{6a}$$

$$\alpha = \frac{1}{\text{tr}(Q_H) + \sum_{i=1}^{2} w_{H,i}}. \tag{6b}$$

Equations (7) and (8) represent the OCP and the stage cost function $l_{L,i}$ of the LeMPC, respectively

$$\underset{\boldsymbol{u}_h, \boldsymbol{u}_l}{\text{minimize}} \quad \sum_{i=1}^{n_L} l_{L,i}(\boldsymbol{y}_i, \boldsymbol{u}_i; \boldsymbol{\rho}) \tag{7a}$$

$$\text{s.t. } (2), (1), (3b), (3c), (4) \tag{7b}$$

$$p_{2,0} = p_{2,\text{mea}}, \quad x_{O,0} = x_{O,\text{est}} \tag{7c}$$

$$\tilde{u}_{h,0} = \tilde{u}_{h,\text{mea}}, \quad \tilde{u}_{l,0} = \tilde{u}_{l,\text{mea}} \tag{7d}$$

$$u_v = u_v^*(1) \tag{7e}$$

$$\boldsymbol{u}_{h,\text{min}} \leq \boldsymbol{u}_h \leq \boldsymbol{u}_{h,\text{max}}, \quad \boldsymbol{u}_{l,\text{min}} \leq \boldsymbol{u}_l \leq \boldsymbol{u}_{l,\text{max}} \tag{7f}$$

$$\boldsymbol{x}_{\text{min}} \leq \boldsymbol{x} \leq \boldsymbol{x}_{\text{max}} \tag{7g}$$

$$\lambda_O \geq \lambda_{O,\text{min}}$$

$$k \in \{0, 1, \dots, n_L - 1\} \tag{7h}$$

where

$$
\begin{aligned}
l_{L,i} := \beta \times \Big\{ & \left(\boldsymbol{N_y y_i}\right)^{\mathrm{T}} \boldsymbol{Q_L} \left(\boldsymbol{N_y y_i}\right) \\
& + w_{L,1}\left(N_{u_h} u_{h,i}\right)^2 + w_{L,2}\left(N_{u_l} u_{l,i}\right)^2 \\
& + w_{L,3}\left(N_{\Delta u_h} \Delta u_{h,i}\right)^2 + w_{L,4}\left(N_{\Delta u_l} \Delta u_{l,i}\right)^2 \Big\}
\end{aligned}
\tag{8a}
$$

$$\beta = \frac{1}{\text{tr}(\boldsymbol{Q_L}) + \sum_{i=1}^{4} w_{L,i}}. \tag{8b}$$

The stage cost functions (6) and (8) penalize the variation and the energy of valve positions. The operating point specific, most efficient VNT valve position $u_{v,\text{eff}}$ is used to operate VNT efficiently and away from choking and surging boundaries. This, however, does not guarantee the satisfaction of choking and surging boundaries. Instead, they are enforced with box constraints in (5e) using LUTs that are operating point specific and provided as-is from FEV GmbH. The control variations as well as the energy of each valve are penalized with very small weightings during tuning (see Section IV). The energy saving of valve actuation is insignificant compared to the overall engine efficiency. However, these penalizations are useful to gradually recover valve positions to a nominal placement (i.e., toward 0% for EGRs and v_{eff} for VNT) at steady loadings such as idling.

The HeMPC computes the optimal VNT valve position trajectory and oxygen concentration. The LeMPC receives $u_v^*(1)$ in (7e) and assumes that it stays constant for the prediction horizon. Meanwhile, the optimal trajectory of oxygen concentration computed by HeMPC is discarded.

Both OCPs exploit the limit on λ_O for the tracking of torque since the satisfaction of (5g) and (7h) allows sufficient fuel to deliver the demanded torque. The λ_O limits are enforced as soft constraints that allow minor violations. This ensures that the OCPs are feasible during rapid increase of torque demand.

Solving (5) and (7) requires the HeMPC and LeMPC to agree on an optimal tradeoff between boost pressure and in-cylinder oxygen. Due to the emission tradeoff, a NOx-favored HeMPC will work against a soot-favored LeMPC, causing systematic degradation of performance. A similar weighting of Q_h and Q_L is sufficient to prevent these conflicting emission objectives as the oxygen concentration, controlled by LeMPC, has a dominant effect on emissions.

The normalization factors $N_{(\cdot)}$ are dependent on the range of signals and the engine. α and β normalize weightings to form a convex combination of objectives in (6) and (8).

TABLE I

HARDWARE SPECIFICATIONS OF THE SIMULATION AND HIL PLATFORMS

	Desktop	A80Q7 evaluation board [41]
Used for	Simulation Study	HiL
Hardware Detail	Intel Xeon E5-1620 CPU (3.60 GHz), 12GB RAM.	8 cores, including 4xARM Cortex -A15 (1.2 GHz) and 4xARM Cortex-A7 (0.48 GHz), 2GB RAM.
OS	Win10 Pro 64-bit	Linux Debian 'Jessie' 32-bit
Controller Program	Double precision, single thread.	Double precision, single thread on Cortex-A15.

TABLE II

WEIGHTINGS $w_{(\cdot)}$ AND $Q_{(\cdot)}$ USED IN THE HEMPC AND LEMPC

Weights	Objective Function Term	L	M	H	EH
Q_H	$x_{nox,H}^2$	0.600	0.800	1.000	1.000
	$x_{soot,H}^2$	3.000	2.000	1.000	0.950
	$p_{loss,H}^2$	0.095	0.150	0.098	0.018
$w_{H,1}$	$(u_v - u_{v,\text{eff}})^2$	0.090	0.050	0.050	0.200
$w_{H,2}$	$(\Delta u_v)^2$	0.100	0.100	0.100	0.500
Q_L	$x_{nox,L}^2$	0.851	1.400	0.810	0.910
	$x_{soot,L}^2$	3.000	3.000	1.000	1.000
	$p_{loss,L}^2$	0.080	0.030	0.040	0.060
$w_{L,1}$	u_h^2	0.001	0.001	0.001	0.001
$w_{L,2}$	u_l^2	0.002	0.002	0.001	0.001
$w_{L,3}$	$(\Delta u_h)^2$	0.050	0.150	0.070	0.010
$w_{L,4}$	$(\Delta u_l)^2$	0.050	0.150	0.070	0.010

IV. ONLINE IMPLEMENTATION OF THE CONTROLLERS

The controllers' performance and execution efficiency are evaluated on a desktop PC and an HiL implementation using the A80Q7 evaluation board [41] in-loop with a dSPACE SCALEXIO system [42]. Table I presents the hardware specifications. The controller runs over the WLTC, which contains four duty stages, namely, light (L), medium (M), heavy (H), and extra-heavy (EH). The performance criteria are NOx and soot in mass and brake specific form, mean BSFC, and torque demand tracking error in RMSE.

The controller improves on the base solver described in [19] by using a gradient descent approach when backtracking line search method fails. This reduces the computational overhead to check for the unlikely occurrence of NPD Hessian matrix, which occurs in only 4.41% and 0.03% of the WLTC for HeMPC and LeMPC, respectively, using desktop simulation.

The HeMPC and LeMPC are tuned for each duty stage of the WLTC, as shown in Table II. The tuning has been designed in reference to the eMPC [19] to focus on NOx and soot emissions while providing good torque tracking without degrading the fuel economy. Each satisfactory manual tuning serves as an initial guess for a gradient descent routine to search automatically for finer improvements in adjacent areas. The tuning of NOx and soot mainly depends on LeMPC due to emission being more sensitive to oxygen concentration than to boost pressure. The tuning of pumping loss penalty depends more on HeMPC for its control over boost pressure in the long term. A heavier duty cycle requires greater emphasis on NOx reduction against soot and lower weight on pumping loss. This shift is due to the heavier duty cycle requiring more oxygen

This article has been accepted for inclusion in a future issue of this journal. Content is final as presented, with the exception of pagination.

LIU et al.: HIERARCHICAL eMPC THAT EXPLOITS LOOK-AHEAD INFORMATION 7

TABLE III

PERFORMANCE IMPROVEMENT (%) BY THE LAeMPC OVER THE LIGHT (L), MEDIUM (M), HEAVY (H), AND EXTRA-HEAVY (EH) STAGES OF WLTC AGAINST THE PRODUCTION-LINE CONTROLLER AND THE eMPC IN [19]. ALL RESULTS EXCLUDE ENGINE IDLING

WLTC Stage	Improvement (%) against Production-Line Controller						Improvement (%) against eMPC w/o Look-Ahead Info in [19]					
	NOx Mass (g)	Soot Mass (g)	BS NOx (g/kW)	BS Soot (g/kW)	Mean BSFC (g/kW)	Torque Tracking RMSE ($\sqrt{\text{Nm}}$)	NOx Mass (g)	Soot Mass (g)	BS NOx (g/kW)	BS Soot (g/kW)	Mean BSFC (g/kW)	Torque Tracking RMSE ($\sqrt{\text{Nm}}$)
Desktop Simulation												
L	16.3	20.3	16.8	20.8	1.0	17.7	5.9	13.4	6.0	13.5	-0.0	2.3
M	11.5	17.8	12.3	18.4	0.7	29.8	10.2	17.4	10.4	17.5	-0.0	3.2
H	7.2	9.4	8.2	10.4	1.7	41.1	4.1	5.5	4.3	5.8	-0.0	10.6
EH	1.3	15.1	1.5	15.2	1.2	28.7	-0.7	13.4	-0.4	13.6	0.4	20.8
Total	**9.2**	**14.4**	**9.7**	**14.9**	**1.2**	**30.9**	**5.3**	**11.5**	**5.5**	**11.7**	**0.1**	**11.1**
HiL Implementation												
L	15.0	31.9	15.0	31.9	1.0	5.0	6.0	10.2	6.0	10.2	0.0	2.1
M	10.7	25.5	10.6	25.4	0.5	-3.6	10.4	19.9	10.2	19.7	-0.1	-5.9
H	9.8	14.7	9.4	14.3	1.5	-6.7	5.2	6.1	5.4	6.3	-0.2	6.6
EH	3.8	15.3	3.7	15.2	1.2	1.4	4.4	6.8	4.5	6.9	0.1	23.7
Total	**9.9**	**20.2**	**9.7**	**20.1**	**1.1**	**-1.2**	**6.8**	**10.3**	**6.8**	**10.3**	**-0.0**	**8.0**

mass and hence higher oxygen cylinder concentration, leading to greater NOx production than soot in their tradeoff relation. Meanwhile, the weighting on pumping loss is eased in order to meet more challenging engine loads. Weightings for control variation and energy are kept nonzero but of very small value initially, followed by automatic adjustments capped by some manually set small values. Multiple initial guesses are used. These weightings may be adjusted to meet a different test cycle based on engine loads and require an adaptive scheme for future works.

All controllers run at 0.01 s with a warm engine start (coolant at 90 °C) and a cold SCR (20 °C) to minimize engine behavior changes due to warming-up across WLTC while retaining a typical engine start for EATS. During idling, all controllers use zero EGR. $u_{v,\text{eff}}$ is set to a constant value throughout the WLTC for simplification. All scaling factors $N_{(\cdot)}$ and $\lambda_{\min}$ are also set to constant values. The states and EGR positions are limited with fixed and compact ranges. The minimum and maximum positions of the VNT are determined using LUTs.

Fig. 4 shows the HiL setup to implement and evaluate the proposed controller for real-time application. The SCALEXIO system running the plant model communicates with the A80Q7 board hosting the controller with a CAN bus at a rate of 1000 kbits/s. Each CAN packet contains up to 8 bytes of payload with a single byte per signal. The controller receives 20 feedback readings as three CAN packets and sends eight control signals carried by one CAN packet. This generates approximately 4% busload. The feedback signals include a counter value sent by the host to indicate the progress of the WLTC. The controller uses the counter value to select weighting and read the look-ahead information, namely, the future speed and torque demand of the engine, from a locally stored array. The entire engine control software runs on a dedicated Cortex-A15 core of the A80Q7 board.
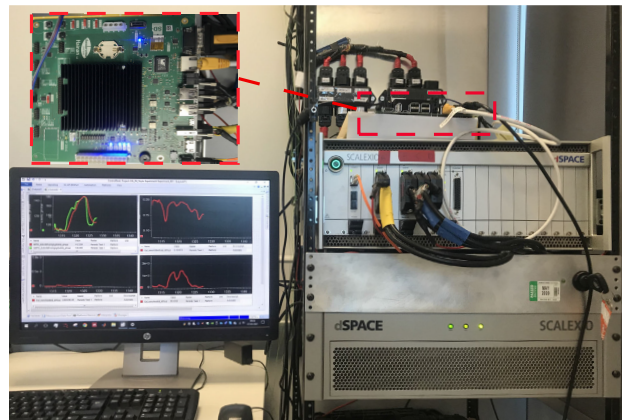

Fig. 4. Photograph of the HiL bench including the SCALEXIO host computer and A80Q7 board (highlighted by dashed boxes). The A80Q7 board is connected to the SCALEXIO via CAN bus. The signals displayed on screen in real time (starting from top left and in clockwise order) are intake/exhaust manifold pressure, in-cylinder oxygen concentration, exhaust manifold soot, and NOx concentration.

V. RESULTS AND DISCUSSION

A. Simulation Study

Table III summarizes the emissions, fuel consumption, and torque tracking results of the engine with the proposed controller compared to an eMPC that does not take look-ahead information into account and a production-line controller. Table III excludes the data during engine idling due to possible start–stop strategy. Compared to the production-line controller, the LAeMPC improves engine performance in every aspect. It allows higher soot reduction than the eMPC. It improves torque tracking steadily as the duty cycle becomes heavier as it exploits the look-ahead information to prepare ahead for larger load variation in heavier duty cycles.

Fig. 5 shows the selected transients from the H and EH parts of WLTC acquired from simulation and HiL. Upon each deceleration event, the LAeMPC achieves up to 5%

This article has been accepted for inclusion in a future issue of this journal. Content is final as presented, with the exception of pagination.

8   IEEE TRANSACTIONS ON CONTROL SYSTEMS TECHNOLOGY
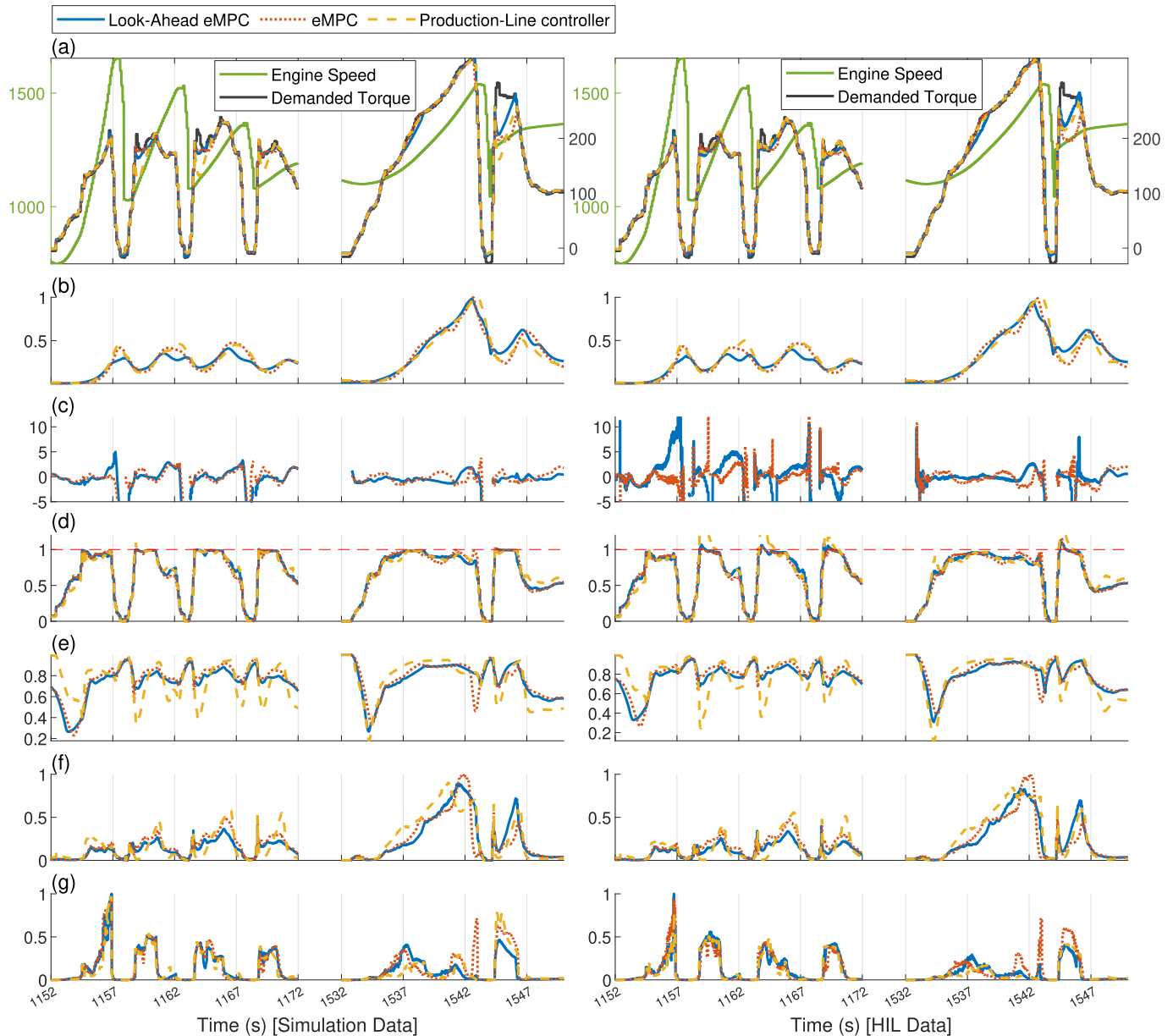

Fig. 5. H and EH duty part of the WLTC time series for a manual transmission engine, with desktop simulation (left) and HiL (right). (a) Engine speed (r/min) (left axis) and torque (Nm) (right axis). (b) Boost pressure. (c) Difference of net indicated efficiency (%) against production-line controller (positive = better). (d) $(\lambda_O)^{-1}$ (OFR over stoichiometric value)$^{-1}$. (e) Cylinder oxygen concentration before combustion. (f) Engine out NOx mass. (g) Engine out soot mass.

higher net indicated efficiency by decreasing the boost pressure earlier (e.g., at 1159 and 1162 s) than the other controllers. During rapid fall-and-rise of the torque demand at 1545 s, the LAeMPC maintains the boost pressure and allows more air intake than the other controllers. As a result, the engine delivers more torque when the demanded torque increases rapidly and hence improves torque tracking. LAeMPC also uses look-ahead information to build up the boost pressure to be just adequate. Between 1155 and 1172 s, all controllers have a similar build-up of boost pressure initially, and however, the LAeMPC relaxes the boost earlier without compromising torque tracking. The proactive relaxation of boost pressure allows the engine to achieve higher indicated efficiency when possible and results in better fuel economy. In terms of emissions, the production-line controller shows an undershoot

tendency in oxygen concentration which causes soot spikes, while the eMPC uses EGR mildly. The undershoot tendency is due to the conservative control strategy adopted by the controller that was optimized based on the magnitude of engine load change. Both LAeMPC and eMPC have kept $(\lambda_O)^{-1}$ under the threshold, but LAeMPC achieves a slightly lower in-cylinder oxygen (e.g., at 1166 s). The lower oxygen value reduces the generation of NOx, at a negligible cost of soot, but is infeasible to eMPC. The production-line controller shows mild violations of $(\lambda_O)^{-1}$ [Fig. 5(f)] since it cuts fuel reactively.

A predictive controller can benefit from the sharp falls and rises of torque by gear shifting to particularly improve the NOx emission and torque tracking. Automatic transmission reduces the engine load transients and may reduce the benefits. The
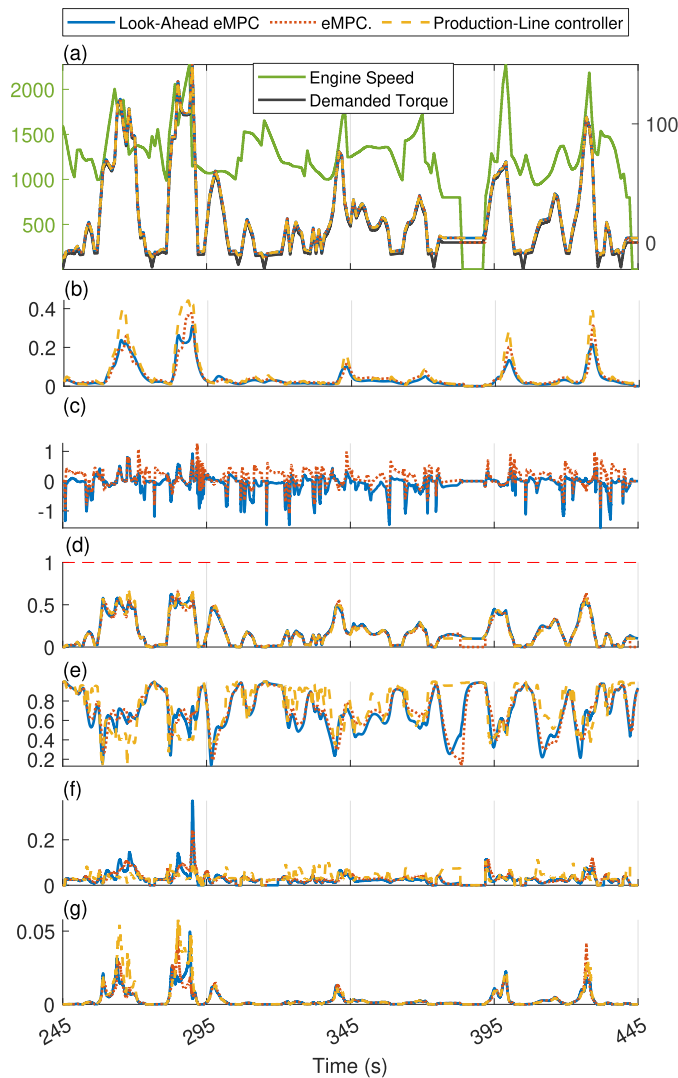
Fig. 6. WLTC time series for an automatic transmission which has fewer transients than a manual transmission. The LAeMPC demonstrates over 8% and 9% improvement for NOx and soot against the eMPC while having similar fuel economy. (a) Engine speed (r/min) (left axis) and torque (Nm) (right axis). (b) Boost pressure. (c) Difference of indicated efficiency (%) against reference controller (positive = better). (d) $(\lambda_O)^{-1}$ (OFR over stoichiometric value)$^{-1}$. (e) Cylinder oxygen concentration before combustion. (f) Engine out NOx mass. (g) Engine out soot mass.

LAeMPC is additionally verified using a WLTC dataset for an automatic transmission with start–stop strategy (see zero engine speed at 385 s in Fig. 6). The production-line controller shows less undershoots of in-cylinder oxygen concentration and smaller differences in indicated engine efficiency. Compared to the other two, the LAeMPC allows lower boost pressure at peak torques [see 265 and 290 s of Fig. 6(b)]. In addition, it shows more proactive control of in-cylinder oxygen concentration than the eMPC. Even for automatic transmission engine, LAeMPC still demonstrates a consistent improvement of 7.2%, 0.1%, 8.3%, and 9.8% in torque tracking, fuel economy, NOx, and soot emissions, respectively, against the eMPC.

The ability of LAeMPC to accommodate uncertainties in look-ahead information, introduced through random time delays and multiplicative noise, is also evaluated using
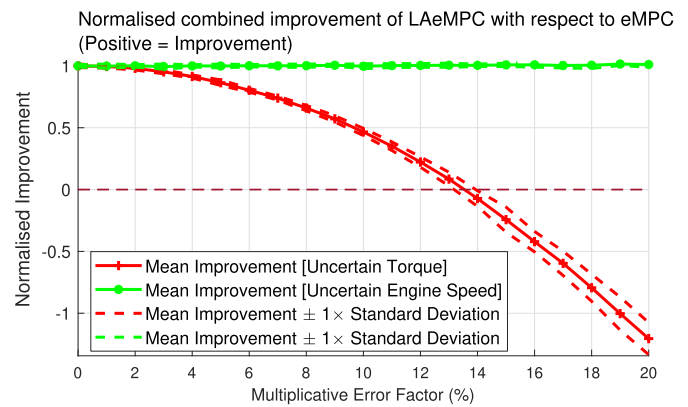

Fig. 7. Normalized combined advantage of LAeMPC against the eMPC from [19], using criteria including emissions, fuel economy, and torque tracking. The simulations use manual transmission and are repeated ten times at each error factor. The controller performance degrades logarithmically with an increase in delays and multiplicative error associated with the look-ahead data of engine speed and torque, respectively. Uncertainty in torque prediction has a dominant effect on performance degradation.

a simulation study. The time delay is a random value from 0 to 2 s following uniform probability distribution. The multiplicative noise is of zero-mean Gaussian distribution with SD proportional to the range of engine speed and torque and resembles the prediction error during transients [38]. The multiplicative factor increments from 0% to 20% to match the worst case RMSE for the predictors in [37] and [38]. Fig. 7 presents the combined advantage of LAeMPC against the eMPC with increasing uncertainty of predicted engine speed and torque. The combined advantage sums the equally weighted percentage improvements of all criteria, each normalized by their value at zero uncertainty. Fig. 7 shows that torque prediction uncertainty dominates the performance degradation, and the LAeMPC retains its benefits up to a 13% multiplicative error factor, with random time delays. This tolerance suggests that the benefits are feasible with predictors in [37] where prediction error can be controlled confidently under 10% mean absolute percentage error. In addition, realistic WLTC involves a driver or some automatic controller to meet the required velocity profiles, forming a loop that results in variant engine speed and loading depending on the engine control performance. However, this work focuses on the evaluation of the engine airpath controllers and assumed an invariant engine speed and torque as a basis for performance comparison. The difference in engine speed and torque due to the human or automatic controllers may be accounted for by the introduction of the aforementioned prediction uncertainties.

Finally, while this study focuses on engine-out emissions, the LAeMPC desktop simulation also demonstrated 4.6% and 8.7% tail-pipe NOx mass reduction over the WLTC compared to the eMPC and production-line controller, respectively, using the same EATS controller while consuming less AdBlue by mass. The resulting temperature profile of SCR is similar in light duty cycles, while eMPC and LAeMPC give slightly higher temperatures at heavier WLTC duty cycles. The accumulation of soot and regeneration of DPF is not considered in this study for their longer horizon related to the temperature dynamics.

This article has been accepted for inclusion in a future issue of this journal. Content is final as presented, with the exception of pagination.

10   IEEE TRANSACTIONS ON CONTROL SYSTEMS TECHNOLOGY

TABLE IV
EXECUTION TIME FOR ENTIRE ENGINE CONTROL SOFTWARE ON CORTEX
A-15 (1200 MHz) ON HiL IMPLEMENTATION

Included airpath controller	Production-line Controller	LAeMPC	eMPC in [19]
Best Case (ms)	0.27	2.83	1.60
Worst Case (ms)	1.20	8.92	9.64
Median (ms)	0.33	5.16	3.64
Mode (ms)	0.32	2.84	2.54
Mean (ms)	0.34	5.01	4.38
SD (ms)	0.03	1.08	2.04

B. HiL Implementation

Table III (lower half) summarizes the results from HiL implementation. The communication between ECU and SCALEXIO employed CAN [43] due to the lack of analog and digital inputs and outputs on the A80Q7 board. The signal precision loss across CAN results in the minor emission performance shift that can be overcome with a slight retuning.

The asynchronous read and write actions between the processor and its CAN controller create an unmodeled transmission latency. The latter adversely affected the estimation of cylinder mass intake and is responsible for a belated fuel cut during rapid torque demand increment. This results in more frequent violation of the $(\lambda_O)^{-1}$ limit compared to the simulation results [see the right half of Fig. 5(e)]. The production-line controller is more sensitive to latency since it cuts fuel reactively. This leads to fuel-rich mixtures resulting in better torque tracking at the cost of higher in-cylinder soot. Both eMPCs are less affected than the reactive controller since OFR is modeled and constrained separately for good torque tracking. This explains the high soot advantage achieved by the LAeMPC compared to the production-line controller (see Table III).

Table IV reports the execution time of the three controllers for ten test runs. The results are consistent with an SD of less than 3% of their respective mean values. The LAeMPC has a shorter worst case execution time and SD than eMPC due to a more efficient numerical solver implementation. While the production-line controller is significantly faster than both MPC, the LAeMPC runs faster than the required 10 ms, at a worst computational time of 8.92 ms. Potential production use of the controller requires more investigations, including the use of explicit MPC [44] or training of deep reinforcement learning controller based on the current design, as well as further algorithmic optimizations such as constraint handling and convexification of the problem.

VI. CONCLUSION

This article has presented a control strategy that exploits look-ahead information of 2 s for the airpath management of a EURO-6 CI engine using manual or automated transmission with stop–start. The proposed controller simultaneously considers engine emissions (NOx and soot), fuel economy, and torque tracking while directly controlling the EGRs and VNT. The approach was first demonstrated using simulation studies and then validated on an HiL implementation. For the

engine associated with a manual transmission, the benefits of look-ahead information are found to improve torque tracking, NOx, and soot emissions by 11.1%, 5.5%, and 11.7%, respectively, with uncompromised fuel economy, compared to another optimal controller without look-ahead information. Compared to a production-line controller for EURO 6 engines, the improvements in torque tracking, NOx, and soot emissions are 30.9%, 9.7%, and 14.9%, respectively, and a 1.2% improvement in fuel economy. The benefits remain consistent when using an automatic gearbox with less aggressive engine transients. Using a Gaussian noise and random time delay, the benefits of look-ahead information degrade gradually and disappear as the SD of the noise increased to approximately 13% of the nominal range of the engine speed and torque over the WLTC. Finally, the LAeMPC is able to meet the execution time required for real-time use with a worst case execution time of 8.9 ms on a 1.2-GHz ARM Cortex-A15 processor. The execution time can be further improved using explicit MPC and optimization of algorithms.

This work shows that look-ahead information, even with random time delays and prediction uncertainty, can benefit airpath control in reducing NOx and soot emissions, at improved torque tracking and fuel economy. A hierarchical formulation of eMPC that splits the control of VNT and EGRs was found useful to harvest a long (2 s) look-ahead horizon while being computationally feasible on a Cortex-A15 core. Future vehicles with greater road awareness, motion planning, and computing hardware may exploit a look-ahead airpath controller to achieve these benefits.

Future works include an adaptive weighting schedule and further on-vehicle validation of the controller where part of the communications will be transferred from the CAN to the digital/analog channels to minimize precision loss and communication latency. Additional works also include choosing a suitable algorithm for look-ahead information prediction and further evaluating the impact of uncertainty on the prediction models.

REFERENCES

[1] T. A. Rajasingham, *Nonlinear Model Predictive Control of Combustion Engines* (Advances in Industrial Control). Cham, Switzerland: Springer, 2021, doi: 10.1007/978-3-030-68010-7.

[2] K. Mollenhauer and H. Tschöke, *Handbook of Diesel Engines*. Berlin, Germany: Springer, 2010.

[3] A. J. Feneley, A. Pesiridis, and A. M. Andwari, "Variable geometry turbocharger technologies for exhaust energy recovery and boosting—A review," *Renew. Sustain. Energy Rev.*, vol. 71, pp. 959–975, May 2017.

[4] S. Park, Y. Kim, S. Woo, and K. Lee, "Optimization and calibration strategy using design of experiment for a diesel engine," *Appl. Thermal Eng.*, vol. 123, pp. 917–928, Aug. 2017, doi: 10.1016/j.applthermaleng.2017.05.171.

[5] A. Pal, Y. Wang, L. Zhu, and G. G. Zhu, "Multi-objective surrogate-assisted stochastic optimization for engine calibration," *J. Dyn. Syst., Meas., Control*, vol. 143, no. 10, pp. 1–10, Apr. 2021, doi: 10.1115/1.4050970.

This article has been accepted for inclusion in a future issue of this journal. Content is final as presented, with the exception of pagination.

LIU et al.: HIERARCHICAL eMPC THAT EXPLOITS LOOK-AHEAD INFORMATION 11

[6] J. Zhang, M. R. Amini, I. Kolmanovsky, M. Tsutsumi, and H. Nakada, "Benefits of feedforward for model predictive airpath control of diesel engines," 2022, *arXiv:2205.05630*.

[7] S. Hong, I. Park, J. Chung, and M. Sunwoo, "Gain scheduled controller of EGR and VGT systems with a model-based gain scheduling strategy for diesel engines," *IFAC-PapersOnLine*, vol. 48, no. 15, pp. 109–116, 2015.

[8] M. Hirata, T. Hayashi, T. Asahi, M. Takahashi, Y. Yamazaki, and S. Kaneko, "Two-degree-of-freedom controller design for diesel engine airpath system considering dynamics of turbocharger and manifolds," *SAE Int.*, vol. 2019, pp. 1–10, Dec. 2019.

[9] J. B. Rawlings, "Tutorial overview of model predictive control," *IEEE Control Syst.*, vol. 20, no. 3, pp. 38–52, Jun. 2000.

[10] A. Norouzi, H. Heidarifar, M. Shahbakhti, C. R. Koch, and H. Borhan, "Model predictive control of internal combustion engines: A review and future directions," *Energies*, vol. 14, no. 19, pp. 1–40, 2021, doi: 10.3390/en14196251.

[11] L. T. Biegler, *Nonlinear Programming: Concepts, Algorithms and Applications to Chemical Processes*. Philadelphia, PA, USA: SIAM, 2010.

[12] M. Huang, K. Zaseck, K. Butts, and I. Kolmanovsky, "Rate-based model predictive controller for diesel engine air path: Design and experimental evaluation," *IEEE Trans. Control Syst. Technol.*, vol. 24, no. 6, pp. 1922–1935, Nov. 2016.

[13] E. R. Gelso and J. Dahl, "Air-path control of a heavy-duty EGR-VGT diesel engine," *IFAC-PapersOnLine*, vol. 49, no. 11, pp. 589–595, 2016.

[14] G. S. Sankar, R. C. Shekhar, C. Manzie, T. Sano, and H. Nakada, "Model predictive controller with average emissions constraints for diesel airpath," *Control Eng. Pract.*, vol. 90, pp. 182–189, Sep. 2019.

[15] D. Liao-McPherson, M. Huang, S. Kim, M. Shimada, K. Butts, and I. Kolmanovsky, "Model predictive emissions control of a diesel engine airpath: Design and experimental evaluation," *Int. J. Robust Nonlinear Control*, vol. 5, pp. 1–32, May 2020.

[16] E. R. Gelso and J. Dahl, "Diesel engine control with exhaust aftertreatment constraints," *IFAC-PapersOnLine*, vol. 50, no. 1, pp. 8921–8926, Jul. 2017.

[17] D. Bergmann, K. Harder, J. Niemeyer, and K. Graichen, "Nonlinear MPC of a heavy-duty diesel engine with learning Gaussian process regression," *IEEE Trans. Control Syst. Technol.*, vol. 30, no. 1, pp. 113–129, Jan. 2022, doi: 10.1109/TCST.2021.3054650.

[18] D. Liao-McPherson, S. Kim, K. Butts, and I. Kolmanovsky, "A cascaded economic model predictive control strategy for a diesel engine using a non-uniform prediction horizon discretization," in *Proc. IEEE Conf. Control Technol. Appl. (CCTA)*, Aug. 2017, pp. 979–986.

[19] Z. Liu, A. M. Dizqah, J. M. Herreros, J. Schaub, and O. Haas, "Simultaneous control of NOx, soot and fuel economy of a diesel engine with dual-loop EGR and VNT using economic MPC," *Control Eng. Pract.*, vol. 108, Mar. 2021, Art. no. 104701.

[20] M. H. C. Garcia et al., "A tutorial on 5G NR V2X communications," *IEEE Commun. Surveys Tuts.*, vol. 23, no. 3, pp. 1972–2026, 3rd Quart., 2021, doi: 10.1109/COMST.2021.3057017.

[21] R. Roriz, J. Cabral, and T. Gomes, "Automotive LiDAR technology: A survey," *IEEE Trans. Intell. Transp. Syst.*, vol. 23, no. 7, pp. 6282–6297, Jul. 2022, doi: 10.1109/TITS.2021.3086804.

[22] C. Eising, J. Horgan, and S. Yogamani, "Near-field perception for low-speed vehicle automation using surround-view fisheye cameras," *IEEE Trans. Intell. Transp. Syst.*, vol. 23, no. 9, pp. 13976–13993, Sep. 2022, doi: 10.1109/TITS.2021.3127646.

[23] F. Ma et al., "Predictive energy-saving optimization based on nonlinear model predictive control for cooperative connected vehicles platoon with V2V communication," *Energy*, vol. 189, Dec. 2019, Art. no. 116120.

[24] M. A. S. Kamal, K. Hashikura, T. Hayakawa, K. Yamada, and J. Imura, "Look-ahead driving schemes for efficient control of automated vehicles on urban roads," *IEEE Trans. Veh. Technol.*, vol. 71, no. 2, pp. 1280–1292, Feb. 2022, doi: 10.1109/TVT.2021.3132936.

[25] J. Wu, H. Zhou, Z. Liu, and M. Gu, "Ride comfort optimization via speed planning and preview semi-active suspension control for autonomous vehicles on uneven roads," *IEEE Trans. Veh. Technol.*, vol. 69, no. 8, pp. 8343–8355, Aug. 2020, doi: 10.1109/TVT.2020.2996681.

[26] D. F. Pereira, F. d. C. Lopes, and E. H. Watanabe, "Nonlinear model predictive control for the energy management of fuel cell hybrid electric vehicles in real time," *IEEE Trans. Ind. Electron.*, vol. 68, no. 4, pp. 3213–3223, Apr. 2021.

[27] G. P. Incremona and P. Polterauer, "Design of a switching nonlinear MPC for emission aware ecodriving," *IEEE Trans. Intell. Vehicles*, vol. 8, no. 1, pp. 469–480, Jan. 2023, doi: 10.1109/TIV.2022.3140484.

[28] C. Huang, R. Salehi, A. G. Stefanopoulou, and T. Ersal, "Hardware-in-the-loop exploration of energy versus emissions trade-off in eco-following scenarios for connected automated vehicles," *Int. J. Engine Res.*, vol. 2022, Jul. 2022, Art. no. 146808742210982, doi: 10.1177/14680874221098212.

[29] D. Velmurugan, T. McKelvey, and D. Lundberg, "Supervisory controller for a light duty diesel engine with an LNT-SCR after-treatment system," *SAE Tech. Papers 2018*, 2018, pp. 1–8.

[30] A. Norouzi et al., "Machine learning integrated with model predictive control for imitative optimal control of compression ignition engines," 2022, *arXiv:2204.00142*.

[31] R. Moriyasu, S. Nojiri, A. Matsunaga, T. Nakamura, and T. Jimbo, "Diesel engine air path control based on neural approximation of nonlinear MPC," *Control Eng. Pract.*, vol. 91, Apr. 2019, Art. no. 104114.

[32] Y. Umezawa, K. Yamauchi, H. Seto, T. Imamura, and T. Namerikawa, "Optimization of fuel consumption and NO X emission for mild HEV via hierarchical model predictive control," *Control Theory Technol.*, vol. 20, no. 2, pp. 221–234, 2022, doi: 10.1007/s11768-022-00097-9.

[33] F. Donatantonio, A. D'Amato, I. Arsie, and C. Pianese, "A multi-layer control hierarchy for heavy duty vehicles with off-line dual stage dynamic programming optimization," *Transp. Res. C, Emerg. Technol.*, vol. 92, pp. 486–503, Jul. 2018, doi: 10.1016/j.trc.2018.05.006.

[34] D. Blanco-Rodriguez, G. Vagnoni, S. Aktas, and J. Schaub, "Model-based tool for the efficient calibration of modern diesel powertrains," *MTZ Worldwide*, vol. 77, no. 10, pp. 54–59, Oct. 2016.

[35] G. Vagnoni et al., "Smart rule-based diesel engine control strategies by means of predictive driving information," *Int. J. Engine Res.*, vol. 20, no. 10, pp. 1047–1058, Dec. 2019.

[36] J. Richenhagen, T. G. Schnorbus, G. Birmes, and H. Pieta, "A modular and scalable software architecture for innovative control functionalities," *Fahrzeug Motorentechnik*, vol. 10, pp. 1309–1328, Jan. 2014.

[37] B. Jiang and Y. Fei, "Vehicle speed prediction by two-level data driven models in vehicular networks," *IEEE Trans. Intell. Transp. Syst.*, vol. 18, no. 7, pp. 1793–1801, Jul. 2017.

[38] J. Shin and M. Sunwoo, "Vehicle speed prediction using a Markov chain with speed constraints," *IEEE Trans. Intell. Transp. Syst.*, vol. 20, no. 9, pp. 3201–3211, Sep. 2019.

[39] S. E. Li et al., "Performance enhanced predictive control for adaptive cruise control system considering road elevation information," *IEEE Trans. Intell. Vehicles*, vol. 2, no. 3, pp. 150–160, Sep. 2017, doi: 10.1109/TIV.2017.2736246.

[40] D. Liao-McPherson, M. Huang, S. Kim, M. Shimada, K. Butts, and I. Kolmanovsky, "Model predictive emissions control of a diesel engine airpath: Design and experimental evaluation," *Int. J. Robust Nonlinear Control*, vol. 2020, pp. 1–32, May 2020.

[41] TheobromaSystems. (2020). *Allwinner Ultraocta A80 Datasheet*. Accessed: Nov. 23, 2020. [Online]. Available: https://www.theobroma-systems.com/wp-content/uploads/2019/06/A80_Datasheet_v1.3_20 150510.pdf

[42] dSPACE. (2020). *Scalexio Modular Real-Time System*. Accessed: Mar. 16, 2021. [Online]. Available: https://www.dspace.com/en/ltd/ home/products/hw/simulator_hardware /scalexio.cfm

[43] P. Dickinson, K. Glover, N. Collings, Y. Yamashita, Y. Yashiro, and T. Hoshi, "Real-time control of a two-stage serial VGT diesel engine using MPC," *IFAC-PapersOnLine*, vol. 48, no. 15, pp. 117–123, 2015.

[44] D. Zhao, C. Liu, R. Stobart, J. Deng, and E. Winward, "Explicit model predictive control on the air path of turbocharged diesel engines," in *Proc. Amer. Control Conf. (ACC)*, 2013, pp. 5213–5218.

Zihao Liu received the B.Eng. degree in automotive engineering and the Ph.D. degree in control engineering from Coventry University, Coventry, U.K., in 2017 and 2022, respectively.

He was a (student) Applied Controls Engineer at Cummins Emission Solutions, Darlington, U.K. He is currently a Control and Algorithm Engineer at YRobot Inc., Suzhou, China, where he works on the control algorithms of wearable robotics. His research focuses on the modeling and optimal control of real-time systems.

Arash M. Dizqah (Member, IEEE) received the M.Eng. degree in electrical engineering from the Sharif University of Technology, Tehran, Iran, in 1998, the M.Sc. degree in electrical engineering from the K. N. Toosi University of Technology, Tehran, in 2001, and the Ph.D. degree in control engineering from Northumbria University, Newcastle upon Tyne, U.K., in 2014.

He was a Research Fellow with the University of Surrey, Guildford, U.K, where he is currently a Senior Lecturer (Associate Professor) in mechanical engineering. He is also the Director of the Smart Vehicles Control Laboratory (SVeCLab), University of Sussex, Brighton, U.K. His research interests lie in control and optimization with applications in vehicles and robotics. He is particularly interested in the real-time implementation of optimization-based control strategies for electrified powertrains, connected and autonomous vehicles (CAVs), and informative path planning with a team of robots.

Jose M. Herreros received the M.Eng. degree in thermal engineering, the M.Sc. degree in chemical, environmental and materials engineering, and the Ph.D. degree in thermal engineering from the University of Castilla-La Mancha, Ciudad Real, Spain, in 2004, 2006, and 2009, respectively, and the M.Sc. degree in motorsport engineering and management from Cranfield University, Cranfield, U.K., in 2010.

He is currently an Associate Professor at the School of Engineering, University of Birmingham, Birmingham, U.K. He has published journal articles on issues related to fuel design and properties, pollutant emissions characterization, and catalysis. His research focuses on the investigation of clean and efficient powertrain systems based on the energy and emission-efficient integration of various propulsion systems with the ultimate goal to develop energy-efficient and clean powertrains to be used in vehicular applications.

Joschka Schaub received the Diploma and Ph.D. degrees in mechanical engineering from RWTH Aachen University, Aachen, Germany, in 2010 and 2015, respectively.

He is currently the Department Manager at FEV Europe GmbH, Aachen, working on control system design for motor and hybrid powertrain applications. He has published journal articles on issues related to new powertrain concepts and advanced control and calibration methods. His research focuses on advanced control system development for energy-efficient and clean powertrains for on-road and off-road applications.

Olivier C. L. Haas (Senior Member, IEEE) received the DUT (Diplôme Universitaire de Technologie) from University Joseph Fourier, Grenoble, France, in 1991, the B.Eng. degree (Hons.) in combined engineering, the M.Sc. degree in control engineering, and the Ph.D. degree from Coventry University, Coventry, U.K., in 1997.

He is currently an Associate Professor in applied control systems and heads the ITS and 5G Group, Centre for Future Transport and Cities, Coventry University. He is a Reviewer for Engineering and Physical Sciences Research Council (EPSRC), U.K., and Plan Cancer, France. He is the Principal Investigator for a commercial project on using deep learning for automated annotation for advanced driver assistance systems. His research interests include multiobjective optimization, control engineering, image processing, and artificial intelligence.

Dr. Haas is on United Kingdom Automatic Control Council (UKACC). For his publications, prizes, and projects, see: https://pureportal. coventry.ac.uk/en/persons/olivier-haas.